Zeitschrift: IABSE reports = Rapports AIPC = IVBH Berichte
Band: 54 (1987)

Artikel: Ultimate load analysis of eccentrically stiffenend shell structures
Autor: Thannon, A.Y. / Bicanic, N. / Owen, D.R.J.
DOI: https://doi.org/10.5169/seals-41944

Ultimate Load Analysis of Eccentrically Stiffened Shell Structures

Calcul à la rupture de structures spatiales raidies

Traglastberechnung von exzentrisch versteiften Schalenkonstruktionen

A.Y. THANNON
Lecturer
University of Mosul
Mosul, Iraq

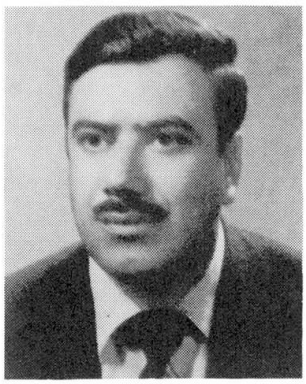

Akram Younis Thannon, born 1941. B.Sc. University of Baghdad, Iraq, 1963. M.Sc. University of Mosul, Iraq, 1978. Worked in design and construction of industrial buildings.

N. BICANIC
Lecturer
University of Wales
Swansea, U.K.

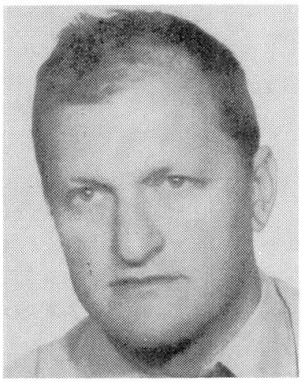

Nenad Bicanic, born 1945. Dipl. Ing. University of Zagreb, Yugoslavia, 1968. Ph.D. University of Wales, 1978. Professor at Faculty of Civil Engineering in Zagreb. He joined the Department in Swansea in 1985.

D.R.J. OWEN
Prof. of Civil Eng.
University of Wales
Swansea, U.K.

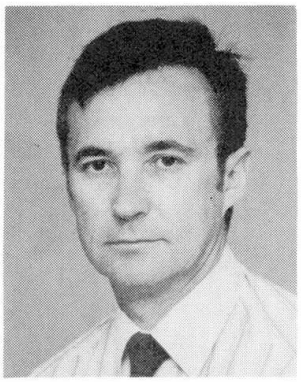

Roger Owen, born 1942. B.Sc., M.Sc., University of Wales. Ph.D. Northwestern University, U.S.A. In 1983 he was awarded the degree of D.Sc. by the University of Wales.

SUMMARY

Numerical solution techniques are presented for simulating the behaviour of reinforced concrete plates and shells stiffened with eccentric beam systems when subjected to short term loading conditions. Degenerate quadratic thick shell elements are employed for the shell and for the beams a curved element formulation is adopted based on beam theory incorporating transverse shear deformation. A through thickness layered representation is used for both the shell and the beam in order to model progressive failure characteristics. Comparison is made with several experimental results.

RÉSUMÉ

Des solutions numériques sont présentées pour la simulation du comportement de plaques et de coques en béton armé raidies avec des systèmes de poutres excentriques, lorsqu'elles sont soumises à des conditions de charges de courte durée. Des éléments de coque épais particuliers sont employés pour la coque tandis qu'une formulation d'éléments courbes est adoptée pour les poutres, sur la base de la théorie des poutres prenant en compte les déformations dues au cisaillement. Une représentation en couches successives est utilisée pour la coque et la poutre afin d'inclure les caractéristiques de la rupture progressive dans le modèle. Une comparaison est faite avec plusieurs résultats expérimentaux.

ZUSAMMENFASSUNG

Numerische Lösungsmethoden werden gezeigt, die das Verhalten von balkenversteiften Stahlbetonplatten und -schalen unter Kurzzeitbelastung simulieren. Entartete quadratische dicke Schalenelemente werden für Schalen verwendet, während für die Balken ein krummliniges Element angewandt wird, das die Schubverzerrung miteinschliesst. Eine über die ganze Dicke reichende Schichtendarstellung wird sowohl für die Schale wie für den Balken gewählt, um fortschreitendes Versagen zu modellieren. Die Ergebnisse werden mit einigen Versuchsresultaten verglichen.

1. INTRODUCTION

The continuing trend towards limit state design of reinforced concrete structures makes increasing demands on the development of adequate computational models for their analysis. The situation is particularly crucial for stiffened shell structures where uncertainties still exist with regards to appropriate element formulation and material modelling under ultimate load conditions. The work presented in this paper represents a further, though small step towards the ultimate goal of a reliable and robust computer code capable of predicting the response of arbitrary stiffened shell structures throughout the entire loading range leading to collapse.

The primary objective of a finite element model developed for global analysis and design purposes is the accurate prediction of the overall deformational and load carrying characteristics of structures together with the corresponding limit loads. The modelling of the complex behaviour of reinforced concrete is frequently simplified in the local context (e.g. crack discontinuities, bond slip) in order to render the problem more tractable and provide numerical solutions within acceptable computational costs. A successful model, however, must be capable of simulating the fundamental nonlinear behaviour up to collapse and must be based on material parameters which can be unambiguously determined from simple tests. The present paper is concerned with developing a numerical approach for modelling the ultimate load response of reinforced concrete shell structures with integral stiffening beams under quasi-static short term loading within these constraints.

The degenerate quadratic thick shell element , employing a layered representation through the thickness, has been successfully employed for the analysis of reinforced concrete plates and shells [1]. Several versions of this element (Lagrangian , Heterosis , Serendipity) have been utilized with various material constitutive models. Most approaches have been based on a dual criterion for yield and crushing in compression expressed in terms of stresses and strains which is complemented with a tension cut-off representation. A smeared or distributed model for cracked concrete is assumed and an average shear modulus is used for cracked zones . Gradual bond deterioration with progressive cracking is simulated by means of a tension stiffening model. Such an approach is again employed in this work as a basis for plate and shell modelling.

The need for a curved beam element to model integral reinforced concrete stiffeners, or even seperate beams, has led to the introduction of various types of elements [2,3] In the present analysis, the curved beam element used by Jirousek [2] for the linear analysis of stiffened shells, is adopted. This element exhibits the required displacement compatibilty with the degenerate quadratic thick shell element. The six degrees of freedom associated with any node are capable of representing torsional and transverse bending behaviour and the element formulation also models transverse shear effects . The constitutive model referred to above must also be modified to allow prediction of the ultimate load behaviour of beam components.

The finite element computational model is summarized and four numerical examples are presented which both illustrate the capabilities of the present code and draw attention to some problems that still exist in the numerical prediction of the ultimate load behaviour of stiffened shell structures.

2. FINITE ELEMENT FORMULATION FOR ECCENTRICALLY STIFFENED PLATES AND SHELLS

2.1 Eccentric curvilinear beam element

2.1.1 Reference, joint and centroidal axes

Fig. 1 illustrates a typical 3 noded curvilinear beam element, with six degrees of freedom comprising three global displacements u_i, v_i, w_i and three global rotations $\alpha_L, \beta_L, \gamma_L$

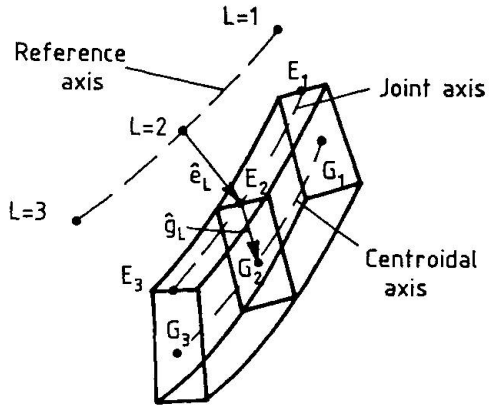

Fig.1 Geometry of the eccentric beam element

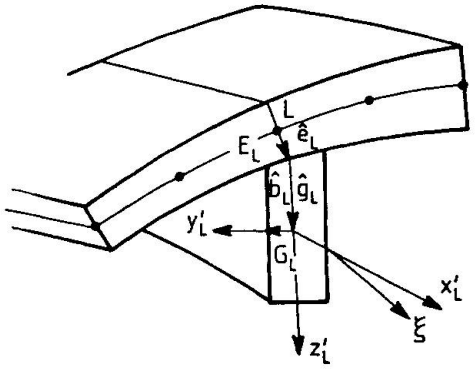

Fig.2 Local coordinate system in a nodal section of the eccentric beam element

The points G1, G2, and G3 are the nodes on the element centroidal axis and ξ is a curvilinear coordinate which varies between (-1,+1). Any point on the element centroidal axis can be defined from

$$\begin{bmatrix} x_G \\ y_G \\ z_G \end{bmatrix} = \sum_{L=1}^{3} N_L(\xi) \begin{bmatrix} x_{GL} \\ y_{GL} \\ z_{GL} \end{bmatrix} \quad \ldots\ldots\ldots\ldots (1)$$

where N_L are the shape functions, and x_{GL}, y_{GL}, z_{GL} are the global cartesian coordinates of the nodes on the element centroidal axis.

When employing such an element in conjuction with a thick shell element to model a stiffened shell, two additional axes have to be introduced, the reference axis, situated at the mid surface of the corresponding thick shell element, and the joint axis on the contact between the beam and the shell, denoted in Fig.1 by points E1,E2 and E3.

Points on the reference axis and on the joint axis can be defined in terms of the corresponding nodal coordinates and the curvilinear coordinate in the same way as points on the centroidal axis are defined in Eq.(1).

The position of the points G_L, E_L with respect to the reference axis can be specified using vectors $\hat{e}_L$, $\hat{g}_L$. Consequently nodal coordinates on the centroidal axis can be expressed in terms of the nodal coordinates on the reference axis as

$$\begin{bmatrix} x_{GL} \\ y_{GL} \\ z_{GL} \end{bmatrix} = \begin{bmatrix} x_L \\ y_L \\ z_L \end{bmatrix} + \hat{e}_L + \hat{g}_L = \begin{bmatrix} x_L \\ y_L \\ z_L \end{bmatrix} + \begin{bmatrix} \Delta x_L \\ \Delta y_L \\ \Delta z_L \end{bmatrix} \quad \ldots\ldots\ldots\ldots (2)$$

The local cartesian coordinates x',y',z' where x' is normal to the plane of the element cross section and y', z' are the principal axes of area of the cross section, are shown in Fig.2 .

The beam cross section at a given ξ should ideally contain point E on the joint axis

$$\begin{bmatrix} x_E \\ y_E \\ z_E \end{bmatrix} = \sum_{L=1}^{3} N_L(\xi) \begin{bmatrix} x_{EL} \\ y_{EL} \\ z_{EL} \end{bmatrix} \quad \text{.....(3)}$$

This requirement cannot be fulfilled in general, if one insists on having the cross section plane rigorously perpendicular to the centroidal axis. It is assumed that the the vector $\hat{b}$ coincides with the direction of the local y'axis so that the cross section plane is approximately normal to the centroidal axis. For intermediate section along the axis it holds that

$$\hat{g}\ (\xi) = \sum_{L=1}^{3} N_L(\xi)\ \hat{g}_L \quad , \quad \hat{b}\ (\xi) = \sum_{L=1}^{3} N_L(\xi)\ \hat{b}_L \quad \text{.....(4)}$$

Using the vectors $\hat{g}$ and $\hat{b}$,the unit vectors in the local coordinate system x,y,z can be computed

$$\hat{i}' = \frac{\hat{a}}{|a|} \quad , \quad \hat{j}' = \frac{\hat{b}}{|b|} \quad , \quad \hat{k}' = \frac{\hat{c}}{|c|} \quad \text{.....(5)}$$

where

$$\hat{a} = \hat{b} \times \hat{g} \quad \text{and} \quad \hat{c} = \hat{a} \times \hat{b} \quad \text{.....(6)}$$

The matrix of the orthogonal transformation from the local to global axes will therefore be given as

$$\Omega\ (\xi) = [\ \hat{i}'(\xi) \quad \hat{j}'(\xi) \quad \hat{k}'(\xi)] \quad \text{.....(7)}$$

2.1.2 Generalized stress-strain relationship.

Assuming that the cross section plane is perpendicular to the centroidal axis, the constitutive equation relating the generalized stress $\underset{\sim}{\sigma}$ (Fig.3) to the generalized strain $\underset{\sim}{\varepsilon}$ will be of the form

$$\underset{\sim}{\sigma} = \underset{\sim}{D}\ \underset{\sim}{\varepsilon} \quad \text{.....(8)}$$

where

$$\underset{\sim}{\sigma} = \begin{bmatrix} N \\ Q_{y'} \\ Q_{z'} \\ M_{y'} \\ M_{z'} \\ T \end{bmatrix} , \quad \underset{\sim}{D} = \begin{bmatrix} EA & & & & & \\ & GA_{y'} & & & 0 & \\ & & GA_{z'} & & & \\ & & & EI_{y'} & & \\ & 0 & & & EI_{z'} & \\ & & & & & GJ \end{bmatrix} , \quad \underset{\sim}{\varepsilon} = \begin{bmatrix} u_{G,x'} \\ v_{G,x'} - \gamma' \\ w_{G,x'} + \beta' \\ \alpha',x' \\ \beta',x' \\ \gamma',x' \end{bmatrix}$$

where , ', denotes the local reference frame and ,x' stands for differentiation with respect to x' .

The cross sectional properties for each layer are

A	cross section area
$A_{y'}$, $A_{z'}$	equivalent shear area
E	modulus of elasticity
G	shear modulus
J	torsional constant
$I_{y'}$,$I_{z'}$	principal moment of inertia

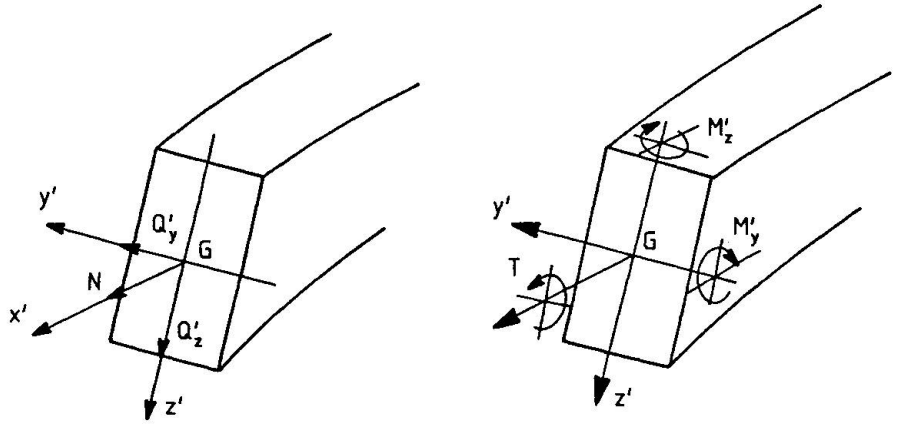

Fig.3 Generalized stress of a curved beam element

The displacements and rotations in the local and global reference system are related through

$$\begin{bmatrix} u'_G \\ v'_G \\ w'_G \end{bmatrix} = \Omega^T \begin{bmatrix} u_G \\ v_G \\ w_G \end{bmatrix} \quad , \quad \begin{bmatrix} \alpha' \\ \beta' \\ \gamma' \end{bmatrix} = \Omega^T \begin{bmatrix} \alpha \\ \beta \\ \gamma \end{bmatrix} \qquad \text{.....(9)}$$

By neglecting the possible small difference between the local axis x' and the tangent to the centroidal axis it follows that

$$\frac{d}{dx'} = \frac{1}{t} \frac{d}{d\xi} \qquad \text{.....(10)}$$

where t is modulus of the vector $\hat{t}$

$$\hat{t}(\xi) = \sum_{L=1}^{3} \frac{dN_L(\xi)}{d\xi} \begin{bmatrix} x_{GL} \\ y_{GL} \\ z_{GL} \end{bmatrix} \qquad \text{.....(11)}$$

2.1.3 Element stiffness matrix

Standard finite element procedures can be followed for computing the stiffness matrix K_G associated with the centroidal axis displacements δ_G

$$K_G = \sum^{Ln} \int_{-1}^{1} B_G^T D B_G \; t \, d\xi \qquad \text{.....(12)}$$

where, Ln is the number of layers through the thickness

The calculation (at the Gauss points) of the strain matrix B_G for each layer follows from

$$\varepsilon = B_G \, \delta_G = \sum_{L=1}^{3} B_{GL} \, \delta_{GL} \qquad \ldots\ldots\ldots\ldots (13)$$

In turn, B_{GL} for each layer can be written by using the definition of the the generalized strain and the transformation matrix Ω as

$$B_{GL} = \begin{bmatrix} \frac{1}{t}\frac{dN_L}{d\xi}\,\Omega^T & \vdots & 0 \\ & \vdots & N_L\,\hat{k}',^T \\ & \vdots & N_L\,\hat{j}',^T \\ \cdots\cdots\cdots\cdots & \vdots & \cdots\cdots\cdots \\ 0 & \vdots & \frac{1}{t}\frac{dN_L}{d\xi}\,\Omega^T \end{bmatrix} \qquad \ldots\ldots\ldots (14)$$

The K matrix associated with the reference axis can be obtained by either transforming K_G matrix or by transforming the strain matrix B from each layer into a strain matrix B_G associated with the reference axis which has been found to be more ecconomical. This latter transformation will be discussed after the formulation of the thick shell element .

2.2 Thick shell element

Formulation of the standard quadratic degenerate shell element (Ahmad's element) is well known [4], and therefore only a brief description of the element will be presented here. Since the element formulation does not allow a direct combination with the beam element described above, the necessary modifications are also summarised.

The degenerate shell element (Fig.4) has five nodal degrees of freedom, i.e three global displacements (u_i, v_i, w_i) and two local rotations (α''_i,β''_i) about the x'' and y'' axes respectively.

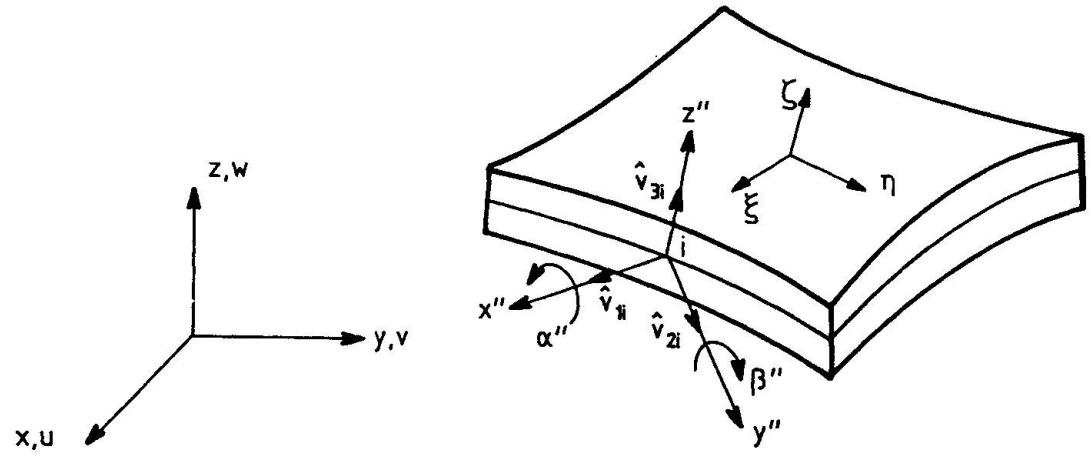

Fig.4 Geometry of a standard thick shell element

The displacement field is assumed to be of the form

$$\begin{bmatrix} u \\ v \\ w \end{bmatrix} = \sum_{i=1}^{n} M_i(\xi,\eta) \begin{bmatrix} u_i \\ v_i \\ w_i \end{bmatrix} + \frac{1}{2} \sum_{i=1}^{n} M_i(\xi,\eta) [-\hat{v}_{2i} \ \hat{v}_{1i}] \begin{bmatrix} \alpha_i'' \\ \beta_i'' \end{bmatrix} \quad ..(15)$$

where x'', y'', z'' are the local coordinate system, $\hat{v}_{1i}$,$\hat{v}_{2i}$,$\hat{v}_{3i}$ are unit vectors and n is the number of nodes.

For the nodes where the shell element is linked to a stiffening beam element, the local rotations (α_L'', β_L'') must be expressed in terms of the global rotations $(\alpha_L, \beta_L, \gamma_L)$

$$\begin{bmatrix} \alpha_L'' \\ \beta_L'' \end{bmatrix} = T_L \begin{bmatrix} \alpha_L \\ \beta_L \\ \gamma_L \end{bmatrix} \quad .....(16)$$

where T_L is a matrix which can be derived from geometric considerations as

$$T_L = \begin{bmatrix} -\hat{v}_{2L}^T \\ \hat{v}_{1L}^T \end{bmatrix} \begin{bmatrix} 0 & v_{3L}^z & -v_{3L}^y \\ -v_{3L}^z & 0 & v_{3L}^x \\ v_{3L}^y & -v_{3L}^z & 0 \end{bmatrix} \quad ...(17)$$

The transformation of the generalized degenerated shell degrees of freedom δ_L'' to δ_L is then given by

$$\begin{bmatrix} u_L \\ v_L \\ w_L \\ \alpha_L'' \\ \beta_L'' \end{bmatrix} = \begin{bmatrix} I & 0 \\ 0 & T_L \end{bmatrix} \begin{bmatrix} u_L \\ v_L \\ w_L \\ \alpha_L \\ \beta_L \\ \gamma_L \end{bmatrix} \quad ...(18)$$

2.3 Beam element combined with the degenerate shell element

To meet the requirements of displacement compatibility along the joint axis, it is assumed that the displacement field of the curved beam element is generated by linking each cross-section to the reference axis by means of a rigid rod vector $\hat{e}_L(\xi)$. It can be shown [2] that

$$\begin{bmatrix} u_{GL} \\ v_{GL} \\ w_{GL} \end{bmatrix} = \begin{bmatrix} u_L \\ v_L \\ w_L \end{bmatrix} + A_L \begin{bmatrix} \alpha_L \\ \beta_L \\ \gamma_L \end{bmatrix} \quad .....(20)$$

where

$$A_L = \begin{bmatrix} 0 & \Delta z_L & -\Delta y_L \\ -\Delta z_L & 0 & \Delta x_L \\ \Delta y_L & -\Delta x_L & 0 \end{bmatrix}$$

The B_{GL} submatrix in Eq. (15) associated with the centroidal axis nodes can be transformed to B_G (associated with the reference axis nodes) by

$$B_L = B_{GL}\, TR_L \qquad \text{.....(21)}$$

where

$$TR_L = \begin{bmatrix} I & \vdots & 0 \\ \cdots & \vdots & \cdots \\ 0 & \vdots & A_L \end{bmatrix}$$

Finally the total stiffness matrix can be assembled following standard finite element procedures.

3. MATERIAL MODELLING

Usually, a simplified formulation of the highly complex behaviour of reinforced concrete is employed [6] and the formulation adopted here has been found very effective despite its simplicity [5].

The compressive behaviour of concrete is modellled using the flow theory of plasticity [8]. Employing Kupfer's results [7], the yield condition for the plate and shell elements is written in stress component form as

$$f(\sigma)=[1.335[(\sigma_x^2+\sigma_y^2-\sigma_x\sigma_y)+ 3(\tau_{xy}^2+\tau_{xz}^2+\tau_{yz}^2)] +0.355\sigma_o(\sigma_x+\sigma_y)]^{1/2} = \sigma_o \qquad \text{.....(22)}$$

This yield condition is a function of only one material parameter ($\sigma_o=f_c'$) which can be obtained relatively easily from experimental data.

The crushing condition is controlled by the state of straining and can be written in terms of total strain components again based on Kupfer's results as

$$1.335[(\varepsilon_x^2+\varepsilon_y^2-\varepsilon_x\varepsilon_y)+ 0.75(\gamma_{xy}^2+\gamma_{xz}^2+\gamma_{yz})] +0.355\ \varepsilon_u(\varepsilon_x+\varepsilon_y) = \varepsilon_u^2 \qquad \text{.....(23)}$$

When ε_u reaches the specified limiting value the concrete is assumed to have lost all its characteristics of strength and stiffness.

For the beam element, the uniaxial behaviour of concrete Fig.5 is adopted.

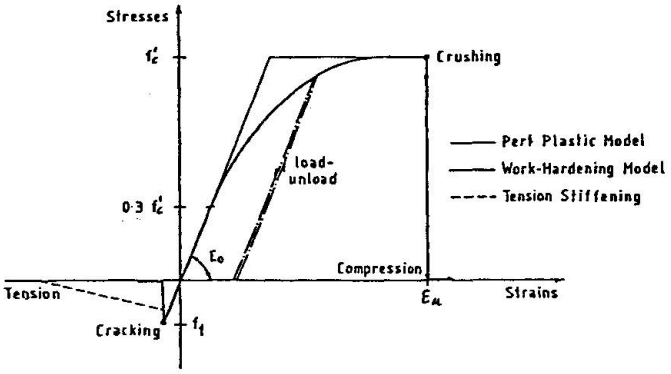

Fig.5 Uniaxial representation of the concrete constitutive model

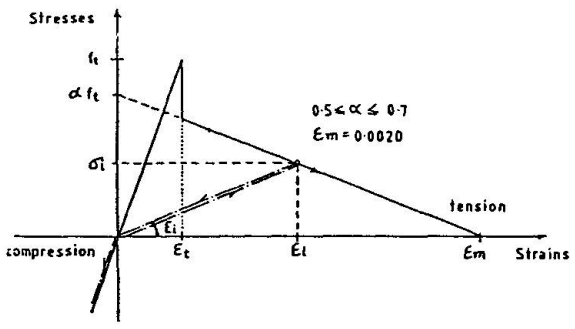

Fig.6 Tension stiffening diagram

The response of concrete under stress is assumed to be linearly elastic until the fracture surface is reached. When the maximum tensile stress is reached, cracks are assumed to form in planes perpendicular to the direction of the maximum principal stress.

After cracking has occured, either a sudden release or gradual relaxation of the normal stress on the cracked plane is adopted according to a tension stiffening diagram as shown in Fig. (6). The modulus of elasticity and the Poisson's ratio are reduced to zero in the direction perpendicular to the crack plane. A reduced shear modulus taken as a function of tensile strain is employed to simulate aggregate interlock.

The behaviour of steel in tension and compression is modelled by considering the reinforcing steel bars as layers of equivalent thickness. Each steel layer has a uniaxial behaviour, i.e resisting only the axial force in the bar direction.

An incremental/iterative numerical solution technique is used in order to trace the response of the structure throughout the loading history. The modified Newton-Raphson method has been employed to avoid frequent calculation and factorization of the tangential stiffness matrix.

4. NUMERICAL EXAMPLES

4.1 Duddeck's two span beam

A simply supported reinforced concrete beam, continuous over two spans tested by Duddeck et al [9] is shown in Fig.7. The material properties as reported by Muller [10] are given in Table 1.

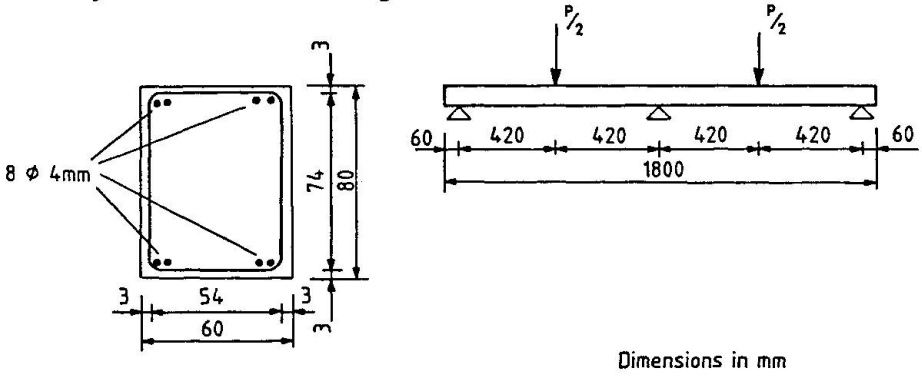

Fig.7 Geometry and details of Duddeck's beam

Table 1 Material properties for Duddeck's beam in (N,mm)

concrete		steel	
Young's Modulus	$E_c = 16660.$	Young's Modulus	$E_s = 196000.0$
Poisson's ratio	$\nu = 0.0$	Young's Modulus	$E_s = 28000.0$
Ult. Comp. St.	$f'_c = 32.0$	Yield Stress	$F_Y = 490.0$
Ult. Tens. St.	$f'_t = 1.67$		
Ult. Comp. Stn.	$\varepsilon_u = .0027$		
Tens. Stiff. Coeff.	$\alpha = 0.5$		
Tens. Stiff. Coeff.	$\varepsilon_m = 0.0015$		

Taking advantage of symmetry only one half of the beam is considered and idealized by 8 beam elements.

Results from the analysis in Fig.8 are in close agreement with experimental observations and data.

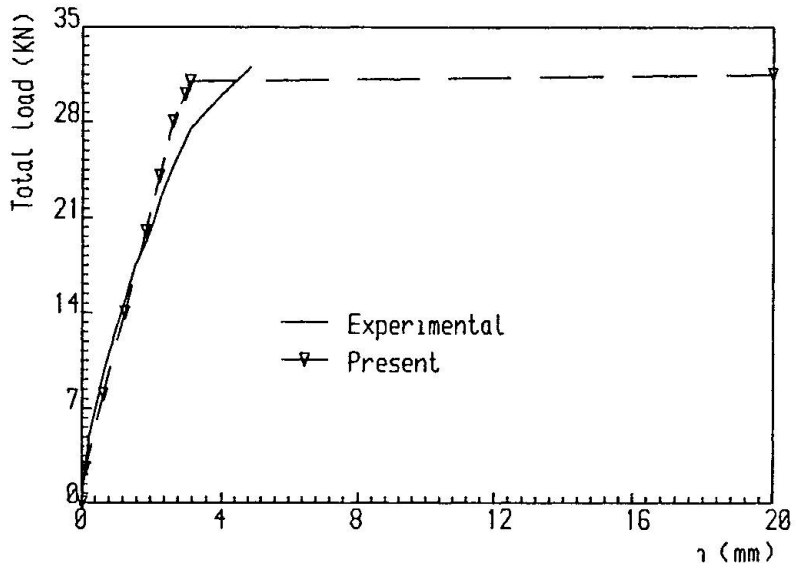

Fig.8 comparison of the load deflection curve for Duddeck's beam.

4.2 Cope and Rao 'T' beam analysis

The reinforced concrete 'T' beam tested by Cope and Rao [11] is chosen to assess the present approach in solving problems involving an assembly of plates and beams. The details of the T beam are shown in Fig.9 , and the relevant material properties are given in Table 2.

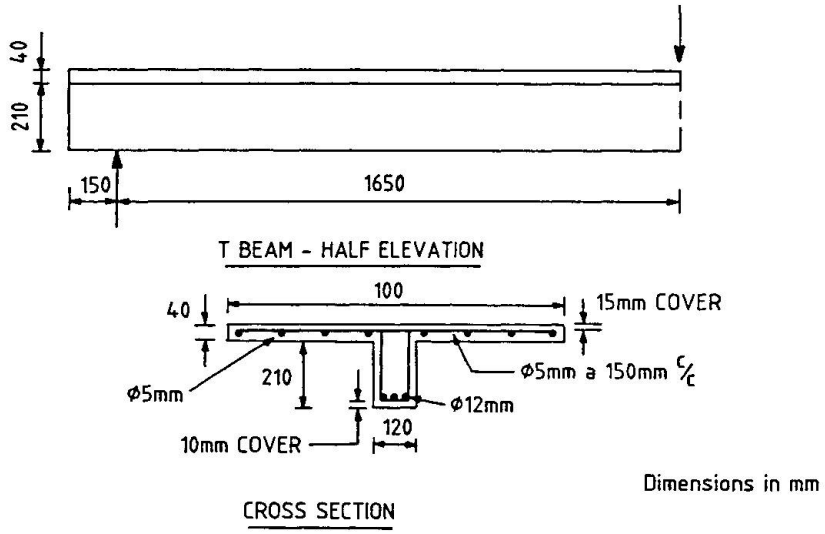

Fig.9 Geometry and details of the Cope/Rao T beam

Table 2 Material properties for Cope/Rao T beam in (N,mm)

concrete		steel	
Young's Modulus	$E_c = 35000.$	Young's Modulus	$E_s = 200000.0$
Poisson's ratio	$\nu = 0.2$	Young's Modulus	$E'_s = 0.00$
Ult. Comp. St.	$f'_c = 48.0$	Yield Stress	$F_Y = 340.0$
Ult. Tens. St.	$f'_t = 4.80$		
Ult. Comp. Stn.	$\varepsilon_u = .003$		
Tens. Stiff. Coeff.	$\alpha = 0.5$		
Tens. Stiff. Coeff.	$\varepsilon_m = 0.0015$		

Using symmetry conditions, one quarter of the T beam is idealized by 12 shell elements and 12 beam elements.

Comparison of the numerical results with those of the experiment in Fig.10 indicates a difference at the initial stage of the response. This difference was also reported by Cope and Rao [11], and can be explained by the existence of micro cracks which reduce the effective tensile strength of the concrete. The close agreement in the later stages up to failure, shows that the present predictive approach is both efficient and adequate. The predicted ultimate load of 36 KN was very close to the experimental load of 40 KN.

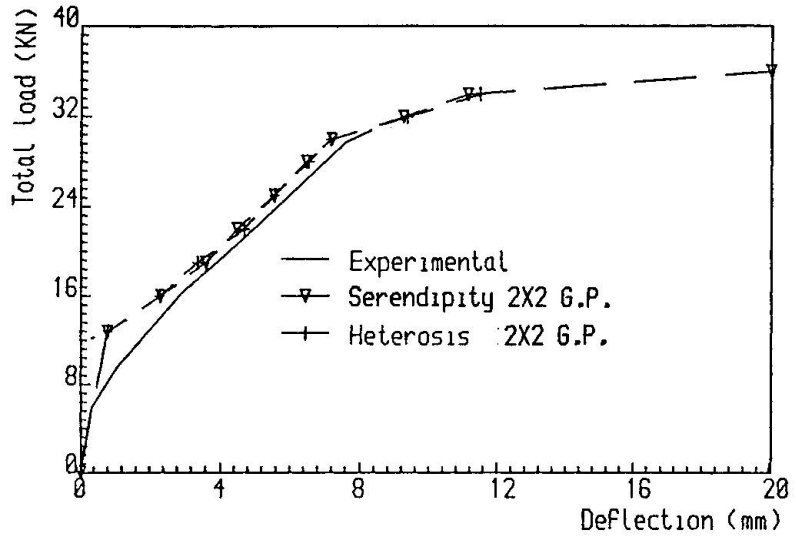

Fig.10 Comparison of load deflection curves for Cope/Rao T beam

4.3 Bouma's cylindrical shell with edge beams

From a series of experimental tests performed on various cylindrical shell roofs [12,13] two tests are chosen for comparison with the present numerical formulation. Fig.11 illustrates the dimensions and reinforcement details of the cylindrical shell and the edge beams. The shell has end diaphragms and is simply supported at the edge of these diaphragms. The shell surface is subjected to uniformly distributed load in the vertical direction with the free edges being subjected to line loading, and both loads are increased in the same ratio during testing.

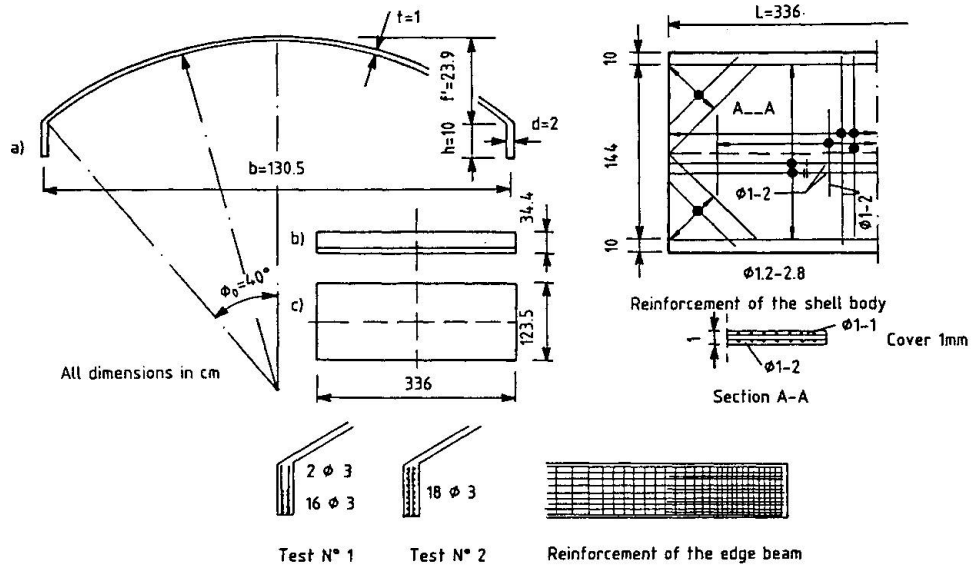

Fig.11 Geometry and details of Bouma's cylindrical shell

For both models, one quarter of the stiffened shell roof has been idealized by 12 shell elements and 4 beam elements, noting the dual symmetry of the problem.

The material properties are assumed to be those indicated in Table 3. The properties are identical to those assumed by both Anerson [13] and Ramm [14] in their analysis of the same shell,which allows comparison with their published predictions.

Table 3 Material properties for Bouma's shells in (N,mm)

concrete		steel	
Young's Modulus	E_c = 30000.	Young's Modulus	E_s = 210000.0
Poisson's ratio	ν = 0.2	Young's Modulus	E_s' = 2000.0
Ult. Comp. St.	f_c' = 30.0	Yield Stress	F_Y = 295.0
Ult. Tens. St.	f_t' = 3.00		
Ult. Comp. Stn.	ε_u = .003	For the edge beam	
Tens. Stiff. Coeff.	α = 0.5		
Tens. Stiff. Coeff.	ε_m = 0.0015	Yield Stress	F_Y = 280.0

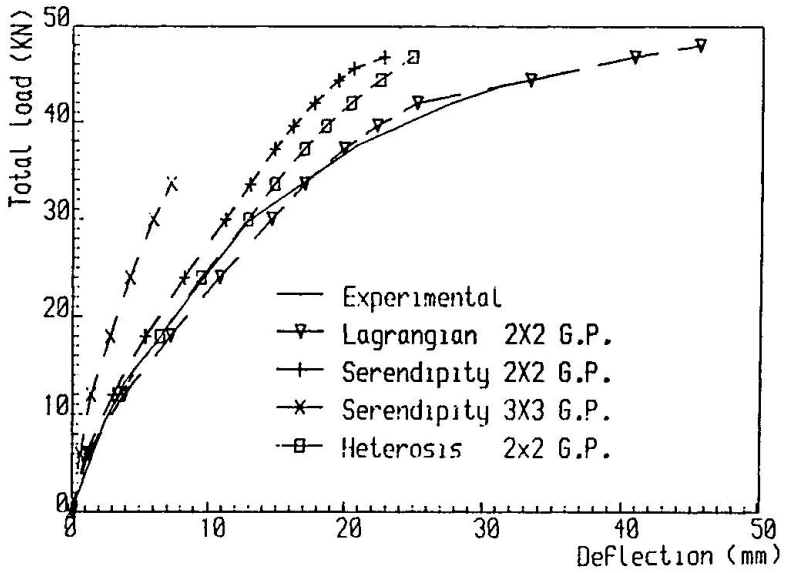

Fig.12 Comparison of load-deflection curves for the middle of the edge beam (Bouma's shell test No.2)

In Fig.12 the numerical results for test No.2 are shown for different types of element and are compared with the test results. The Heterosis element formulation (with reduced integration) shows an excellent agreement with the experimental results up to approximately half the failure load, while the Lagrangian element formulation (with reduced integration) indicates good shell response prediction up to failure load. Full integration leads to a completely 'locked' solution, as expected.

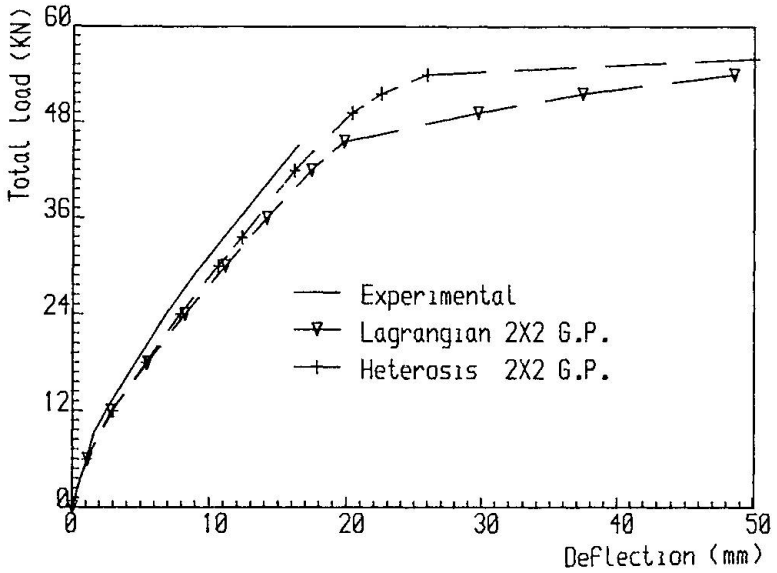

Fig.13 Comparison of load-deflection curves for the middle of the edge beam (Bouma's shell test No.1)

The numerical results for test No.1 are shown in Fig.13. The Heterosis element formulation shows a better agreement with the experimental results than the Lagrangian element formulation.

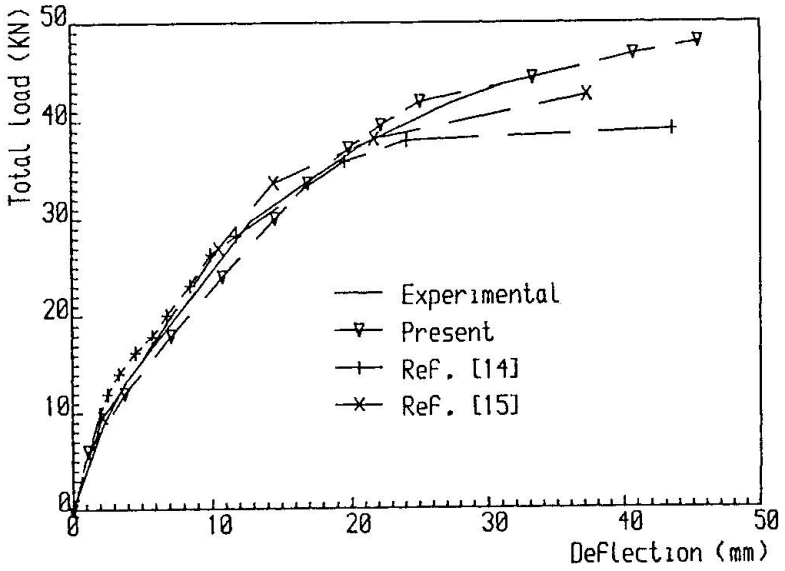

Fig.14 Comparison of load- deflection curves for the middle of the edge beam (Bouma's shell test No.2) with results in Ref. [14,15]

In Fig.14, the numerical results for test No.2 are compared with the predictions from the analyses of Anerson [14] and Ramm [15] and with the experiment results.

It is worth mentioning that in Anerson's analysis the beam was idealized as a shell element connected at it's mid height (inner face) to the shell surface. Ramm [15] also idealized the edge beam as a shell element, and tried 3 different heights of connection point at the middle plane of the beam. The results chosen for comparison here are the best ones reported by Ramm [15]. In addition, both Ramm [15] and Anerson [14] did not mention that the load imposed on the shell during the actual test was composed of two parts, one uniformly distributed on the shell surface and the second being a line load applied to the edge beam, as clearly stated by Bouma et al. [13].

Finally the applicability of the present code is evident from the comparison of the predicted ultimate loads with the experimental values, as shown in Table 4 .

Table 4

	experimental	predicted
Test No.1	53.4 KN	53.0 KN
Test No.2	42.3 KN	46.0 KN

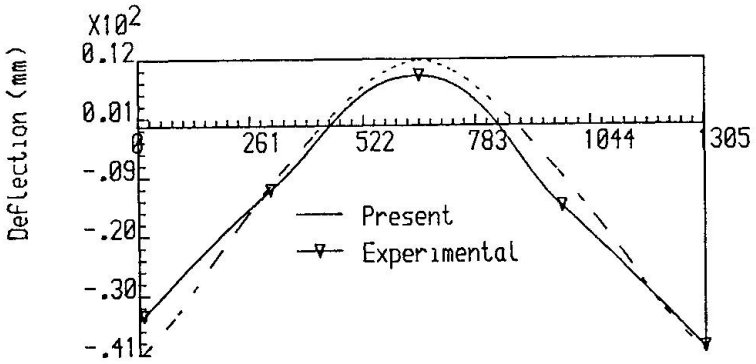

Fig.15 Shell mid section near failure for test No.2

In Fig.15 the shell mid section is shown at different load levels, compared with those measured during test and the very close agreement again illustrates the efficiency of the present approach. The analyses of both Anerson and Ramm did not predict the inward bending of the edge beam and the upward rising of the shell longitudinal centre line.

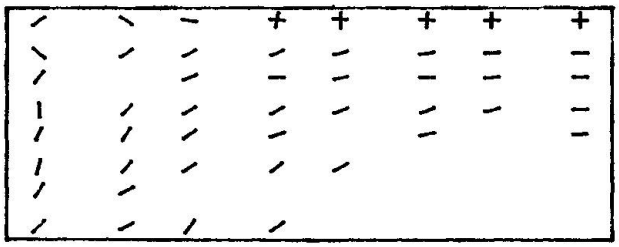

Fig.16 Crack distribution on the upper surface of test No.2

The crack distribution on the upper surface of test No.2 is shown in Fig.16, and is in good agreement with a photograph of the shell taken after failure [12].

5. DISCUSSION AND CONCLUSIONS

A finite element computational model for the ultimate load analysis of stiffened plate and shell structures has been presented and evaluated by application to several problems for which both experimental results and other numerical solutions are available. A good correlation was found between experimental and the present numerical results throughout the entire structural response which demonstrates the effectivness of the solution procedure. The curved beam element, developed to be compatible with degenerate thick shell elements, performed satisfactory and proved to be superior to modelling beam components by additional shell elements.

Further development work is currently being undertaken on the model to include geometric nonlinear effects which have been shown [1] to be significant in the case of unstiffened shells.

Considerable further verification of the solution procedure and associated code is necessary before use in engineering practice can be contemplated.

6. REFERENCES

1. D.R.J. OWEN and J.A. FIGUEIRAS, 'Ultimate load analysis of reinforced concrete plates and shells includung geometrical nonlinear effects', Finite element software for plates and shells, (eds. E. Hinton and D.R.J. Owen), Pineridge press, Swansea, U.K. Sept. 1983.

2. J.JIROUSEK, 'A family of variable section curved beam and thick-shell or membrane-stiffening isoparametric elements', Int.J.num. Meth. Engng, 17,171-186 (1981).

3. G.H. FERGUSON and R.D. CLARK,'A variable thickness curved beam and shell stiffening element with shear deformations',Int.J. num. Meth. Engng, 14 581-592 (1979).

4. S. AHMAD, B.M. IRONS AND O.C. ZEINKEIWICZ, 'Analysis of thick and thin Shell structures by curved elements' Int. J. Num. Engng. 419-451 (1971).

5. J.A. FIGUEIRAS, 'Ultimate load analysis of anisotropic and reinforced concrete plates and shells', Ph.D. Thesis, C/PH/72/83, Department of Civil Engineering, University College of Swansea, U.K. Sept.,1983.

6. W.F. CHEN , 'Plasticity in reinforced concrete', McGraw-Hill book company, New York, 1982.

7. H. KUPFER, K.H. HILSDROF and RUSH, 'Behaviour of concrete under biaxial stresses', Proceedings ACI Vol. 16, No.8, 656-666, 1969

8. D.R.J. OWEN and E. HINTON, 'Finite elements in plasticity, theory and theory and practice', Pineridge Press Ltd. Swansea, U.K. 1980.

9. H.DUDDECK, G. GRIEBENOW, and G. SCHAPER, ' Auszuge aus dem Sechsten Arbeitsbricht zum Forschungsvorhaben Stahlbetonpatten mit nichtlinearen Stoffgesetzen' , Arbeitsbericht Institut fur Statik, TU Braunschweig, 1976.

10. G.MUELLER, 'Numerical problems in nonlinear analysis of reinforced concrete', Report No.UC SESM 77-5, Department of Civil Engineering, University of California, Berkeley, Sept. 1977.

11. R.J COPE and P.V. RAO, ' Nonlinear finite element analysis of concrete slab structures', Proc. Inst. Civil Engng. part 2, 63, 159-197 , 1977.

12. A.C VAN RIEL, W.J. BERANEK and A.C. BOUMA, ' Test on shell roof model roof model of reinforced mortar', Proceedings of 2nd Symposium on concrete shell roof construction, July 1957, Teknisk Ukeblad, Oslo (organized by the Norwegian Engineering Society).

13. A. L. BOUMA, A. C. VAN RIEL, H. VAN KOTEN and W. J. BERANEK, 'Ivestigations on models of eleven cylindrical shells made of reinforced and prestressed concrete', Proceedings of the Symposium on shell research, Delft, Aug. 30 - Sept. 2 1961, (eds. A.M. Haas and A.C. Bouma).

14. A. ANERSEN, 'Analysis of reinforced concrete shells considering material and geometric nonlinearties', Division of structural mechanics, Norwegian Institute of Technology, University of Trondheim, Norway, Report No. 79-1, July 1979.

15. E.RAMM and T.A. KOMPFNER , 'Reinforced concrete shell anlaysis using an inelastic large deformation finite element formulation', Proceeding of the International Conference on computer aided analysis and design of concrete structures, part 1, (eds. F. Damjanic et al.), Pineridge Press, Swansea, U.K. 581-597, 1984.